Chinese Journal of Aeronautics, (2018), 31(6): 1249–1257

Chinese Society of Aeronautics and Astronautics
& Beihang University

Chinese Journal of Aeronautics

cja@buaa.edu.cn
www.sciencedirect.com

Numerical investigation of pyrolysis effects on heat transfer characteristics and flow resistance of n-decane under supercritical pressure

Zhi TAO [a], Xizhuo HU [a], Jianqin ZHU [a,*], Hongwei WU [b]

[a] National Key Laboratory of Science and Technology on Aero-thermodynamics, School of Energy and Power Engineering, Beihang University, Beijing 100083, China
[b] School of Engineering and Technology, University of Hertfordshire, Hatfield AL10 9AB, United Kingdom

Received 10 March 2017; revised 2 August 2017; accepted 25 October 2017
Available online 27 March 2018

KEYWORDS

n-Decane;
Convective heat transfer;
Flow resistance;
Pyrolysis;
Supercritical pressure

Abstract Pyrolysis of hydrocarbon fuel plays an important role in the regenerative cooling process. In this article, a Two-Dimensional (2D) numerical model is proposed to investigate the pyrolysis effects on the heat transfer characteristics and flow resistance of n-decane under supercritical pressure. The one-step global pyrolytic reaction mechanism consisting of 19 species is adopted to simulate the pyrolysis process of n-decane. The thermophysical and transport properties of the fluid mixture are computed and incorporated into the numerical model for simulation. Comparisons between the current predictions and the open published experimental data are carried out and good agreement is achieved. In order to better understand the complicated physicochemical process, further investigations on the turbulent flow and heat transfer coupled with pyrolysis in a tube have been performed under various operating conditions. The results indicate that the pyrolysis intensively takes place in the high fluid temperature region. The occurrence of the heat transfer deterioration would lead to increasing n-decane conversion at the beginning of the heated section. It is found that the pyrolysis could improve the heat transfer deterioration and promote the heat transfer enhancement. Meanwhile, pyrolysis gives rise to an abrupt increase of flow resistance. The mechanisms of the physicochemical phenomena are also analyzed in a systematic manner, which would be very helpful in the development of the regenerative cooling technology.

1. Introduction

Scramjet engines suffer from extremely harsh thermal circumstances, and thus thermal protection to the scramjet engine is becoming a major consideration for hypersonic aircraft. Regenerative cooling has been considered as the most effective and practical method.[1,2] The successful implementation of this

* Corresponding author.
E-mail address: zhujianqinbuaa@sina.com (J. ZHU).

Peer review under responsibility of Editorial Committee of CJA.

Production and hosting by Elsevier

https://doi.org/10.1016/j.cja.2018.03.015

application can lead to greatly improved coolant quality on one hand, and the desired atomization for further efficient combustion on the other hand.[3]

Hydrocarbon fuel is normally injected into the cooling channel under supercritical pressure. During the regenerative cooling process, the hydrocarbon fuel transfers from subcritical to supercritical state as being continuously heated. As a result, the thermal properties would undergo drastic changes when the fuel temperature approaches its pseudo-critical value. Pyrolysis can make the hydrocarbon fuel absorb an extra amount of heat. Meanwhile, the proportions of the fuel components are changed during pyrolysis. All these factors make the flow and heat transfer phenomenon, particularly the heat transfer characteristics, become extremely complicated.[4,5]

Many studies have been devoted to the flow and heat transfer of hydrocarbon fuel under supercritical pressure over the past decades. Hua et al.[6] numerically studied the effects of inlet pressure, inlet velocity, wall heat flux, and the inlet fluid temperature on the supercritical n-heptane heat transfer processes. It was stated that conventional empirical Gnielinski expression could only be used for supercritical heat transfer predictions of n-heptane under very limited operating conditions. Zhou et al.[7] experimentally investigated the mechanism of the heat transfer deterioration of RP-3 at supercritical pressure flowing through vertically downward miniature tubes and a reliable RP-3 heat transfer correlation was developed accordingly. Deng et al.[8,9] conducted an experimental study on RP-3 kerosene in a vertical tube at supercritical pressure. It was found that both the heat flux and flow direction influence the heat transfer characteristics due to buoyancy effect. Urbano and Nasuti[10] carried out a parametric numerical analysis on heat transfer deterioration of supercritical methane, ethane and propane. The correlations for estimating the conditions for the onset of heat transfer deterioration were achieved. We[11] numerically investigated the characteristics of flow resistance and heat transfer of RP-3 at supercritical pressure and it was stated that pressure drop characteristics become diverse under different pressures with a supercritical temperature. Liu et al.[12] performed an experimental study of the convection heat transfer of n-decane at supercritical pressure in vertical tubes. Their results indicated that the buoyancy strongly reduces the heat transfer coefficient in upward flow cases at low inlet Reynolds numbers.

In recent years, researches on pyrolysis of hydrocarbon fuel under supercritical pressure have attracted wide attention. Yu and Eser[13,14] measured the product distributions of C10–C14 normal alkanes thermal decomposition under near-critical and supercritical conditions as well as developed a reaction mechanism. Herbinet et al.[15] improved a previous detailed kinetic model of the thermal decomposition of n-dodecane by measuring the products. Ward et al.[16,17] experimentally investigated the mild-cracking reactions of n-decane and n-dodecane. A Proportional Product Distribution (PPD) model was developed and validated, which is effective for describing the thermal cracking of hydrocarbon fuel. Zhu et al.[18] investigated the flow and heat transfer behavior of the thermal cracking n-decane using a combined experimental and numerical method. The results showed that the second-order reactions increase the proportion of the light products, while decrease the proportion of the heavy products. Zhou et al.[19] measured the heat sinks of n-decane under different pressures and it was found that the effect of the pressure on the endothermicity of n-decane shows different behavior with various temperature ranges. Zhao et al.[20] conducted a numerical simulation for pressure effect on thermal cracking of RP-3. It was observed that increasing pressure would weaken heat transfer when the fuel temperature is above 830 K. Xu and Meng[21] numerically studied the turbulent heat transfer of RP-3 in a micro cooling tube at a supercritical pressure of 5 MPa. Their results indicated that the variation of both the fluid thermophysical properties and the endothermic fuel pyrolysis has significant impact on the heat transfer process for the high fluid temperature region.

The n-decane is one of the main components in many kinds of hydrocarbon fuel.[16] Therefore, a large number of investigations have been carried out on n-decane under supercritical pressure. However, it appears from the previous investigations that rare researches numerically study the flow and heat transfer process of n-decane with the consideration of pyrolysis to obtain a fundamental understanding of the coupled physico-chemical processes in the regenerative cooling tube. As such, the present research is aimed to develop a numerical investigation of the pyrolysis effects on the heat transfer and flow resistance characteristics of n-decane under supercritical pressure. The one-step global pyrolytic reaction mechanism consisting of 19 species is adopted to simulate the pyrolysis process of n-decane. The thermophysical and transport properties of the fluid mixture are calculated and incorporated in the numerical simulation. The pyrolysis process, convective heat transfer and flow resistance under different conditions, as well as the interaction among them, are analyzed in detail.

2. Numerical methods

2.1. Governing equations and solution method

The cylindrical coordinate form of the governing equations for species continuum, momentum, energy and the k-ε turbulence equation can be written as

Continuity equation:

$$\frac{\partial(\rho u Y_i)}{\partial x}+\frac{\partial(\rho v Y_i)}{\partial r}=\frac{\partial J_i}{\partial x}+\frac{\partial J_i}{\partial r}-\frac{\rho v Y_i}{r}+\frac{J_i}{r}+R_i \tag{1}$$

where ρ is the density, Y_i is the mass fraction of species i, J_i is the diffusion flux of species i, and R_i is the mass generation rate of species i due to chemical reaction. u and v are the velocities in axial and radial direction, respectively. x and r are the axial and radial coordinate, respectively.

Momentum equation in the axial and radial directions:

$$\frac{1}{r}\cdot\frac{\partial(r\rho u^2)}{\partial x}+\frac{1}{r}\cdot\frac{\partial(r\rho uv)}{\partial r}=-\frac{\partial p}{\partial x}+\frac{1}{r}\cdot\frac{\partial}{\partial x}\left\{r\mu\left[\frac{\partial u}{\partial x}-\frac{2}{3}\left(\frac{\partial u}{\partial x}+\frac{\partial v}{\partial r}+\frac{v}{r}\right)\right]\right\}+\frac{1}{r}\cdot\frac{\partial}{\partial r}\left[r\mu\left(\frac{\partial u}{\partial r}+\frac{\partial v}{\partial x}\right)\right]+\rho g \tag{2}$$

$$\frac{1}{r}\cdot\frac{\partial(r\rho uv)}{\partial x}+\frac{1}{r}\cdot\frac{\partial(r\rho v^2)}{\partial r}=-\frac{\partial p}{\partial r}+\frac{1}{r}\cdot\frac{\partial}{\partial r}\left\{r\mu\left[\frac{\partial v}{\partial r}-\frac{2}{3}\left(\frac{\partial u}{\partial x}+\frac{\partial v}{\partial r}+\frac{v}{r}\right)\right]\right\}+\frac{1}{r}\cdot\frac{\partial}{\partial x}\left[r\mu\left(\frac{\partial u}{\partial r}+\frac{\partial v}{\partial x}\right)\right]-2\mu\frac{v}{r^2}+\frac{2}{3}\cdot\frac{\mu}{r}\left(\frac{\partial u}{\partial x}+\frac{\partial v}{\partial r}+\frac{v}{r}\right) \tag{3}$$

where p is the pressure, μ is the viscosity, and g is the acceleration of gravity.

Energy equation:

$$\frac{\partial(\rho uH)}{\partial x}+\frac{\partial(\rho vH)}{\partial r}=\frac{\partial}{\partial x}\left(\lambda\frac{\partial T}{\partial x}\right)+\frac{\partial}{\partial r}\left(\lambda\frac{\partial T}{\partial r}\right)-\frac{\rho vH}{r}+\frac{\lambda}{r}\cdot\frac{\partial T}{\partial r}+S \tag{4}$$

where H is the specific enthalpy, T is the temperature, λ is the thermal conductivity, and S is the energy source term due to chemical reaction.

k-ε turbulence equation:

$$\begin{aligned}\frac{\partial(\rho uk)}{\partial x}+\frac{\partial(\rho vk)}{\partial r}=&\frac{\partial}{\partial x}\left[\left(\mu+\frac{\mu_t}{\sigma_k}\right)\frac{\partial k}{\partial x}\right]\\&+\frac{\partial}{\partial r}\left[\left(\mu+\frac{\mu_t}{\sigma_k}\right)\frac{\partial k}{\partial r}\right]-\frac{\rho vk}{r}\\&+\frac{1}{r}\left(\mu+\frac{\mu_t}{\sigma_k}\right)\frac{\partial k}{\partial r}+G_k-\rho\varepsilon\end{aligned} \tag{5}$$

$$\begin{aligned}\frac{\partial(\rho u\varepsilon)}{\partial x}+\frac{\partial(\rho v\varepsilon)}{\partial r}=&\frac{\partial}{\partial x}\left[\left(\mu+\frac{\mu_t}{\sigma_\varepsilon}\right)\frac{\partial \varepsilon}{\partial x}\right]+\frac{\partial}{\partial r}\left[\left(\mu+\frac{\mu_t}{\sigma_\varepsilon}\right)\frac{\partial \varepsilon}{\partial r}\right]\\&-\frac{\rho v\varepsilon}{r}+\frac{1}{r}\left(\mu+\frac{\mu_t}{\sigma_\varepsilon}\right)\frac{\partial \varepsilon}{\partial r}+C_1G_k\frac{\varepsilon}{k}-C_2\rho\frac{\varepsilon^2}{k}\end{aligned} \tag{6}$$

where k is the turbulent kinetic energy, ε is the dissipation rate of k, μ_t is the eddy viscosity, and G_k is the turbulent production due to buoyancy and shear stress. C_1, C_2, σ_k and σ_ε are constants. The governing equations were solved by the Computational Fluid Dynamics (CFD) software FLUENT. The SIMPLEC algorithm was utilized for the pressure field, and the second-order upwind scheme was used to discretize convection terms. The k-ε two-equation model was adopted to simulate the turbulent flow and the "enhanced wall treatment" was employed to determine the near wall velocity, which could well predict the convective heat transfer in the tube.[18,21,22]

2.2. Chemical kinetics model

A one-step PPD chemical model was proposed by Ward et al.[16] based on their experimental measurements. The measured mass fractions of the major decomposed products at different pressures were averaged to obtain a general reaction mechanism.[16]

$$\begin{aligned}C_{10}H_{22}\rightarrow{}&0.151H_2+0.143CH_4+0.256C_2H_4+0.126C_2H_6\\&+0.230C_3H_6+0.180C_3H_8+0.196C_4H_8\\&+0.102C_4H_{10}+0.171C_5H_{10}+0.124C_5H_{12}\\&+0.195C_6H_{12}+0.089C_6H_{14}+0.169C_7H_{14}\\&+0.072C_7H_{16}+0.152C_8H_{16}+0.012C_8H_{18}\\&+0.053C_9H_{18}+0.003C_9H_{20}\end{aligned} \tag{7}$$

The pyrolytic reaction rate of n-decane can be calculated as

$$\frac{d(C_{10}H_{22})}{dt}=-k_c(C_{10}H_{22}) \tag{8}$$

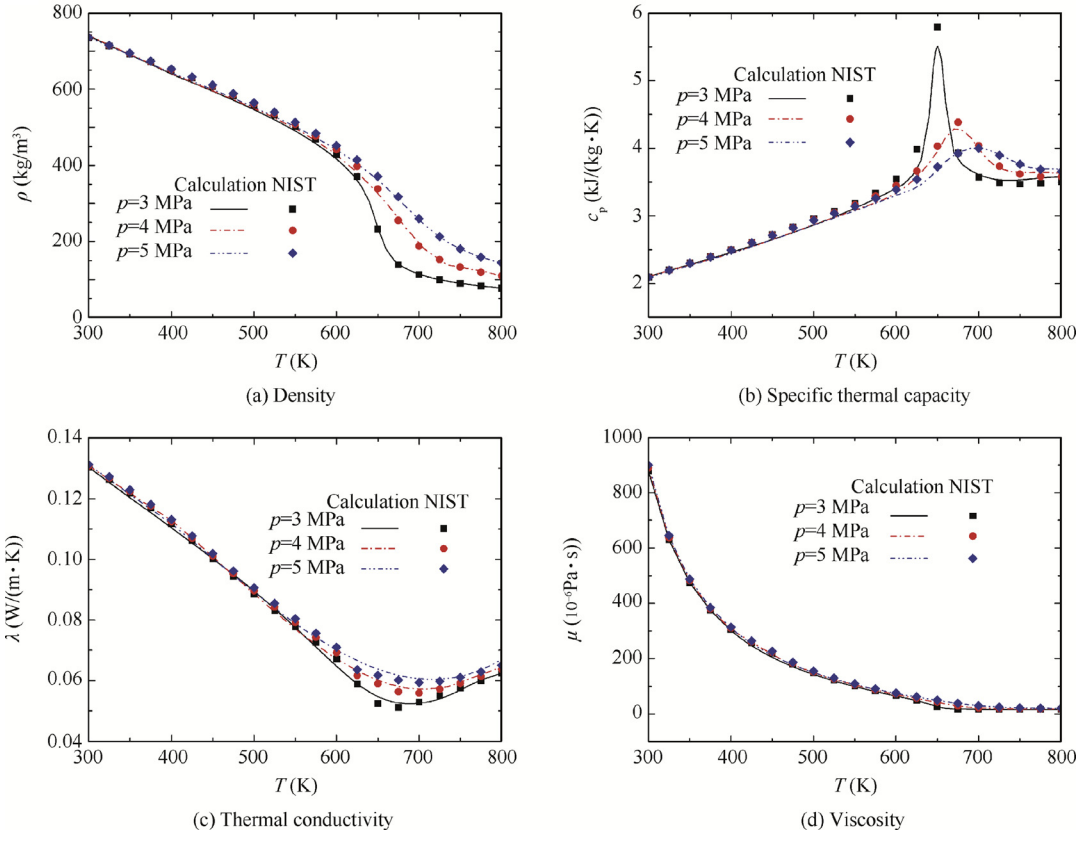

Fig. 1 Validation of calculated thermophysical properties of n-decane.

where the rate constant k_c is computed using the Arrhenius expression

$$k_c = A_c e^{-E/(RT)} \tag{9}$$

The pre-exponential factor $A_c = 1.6 \times 10^{15}$/s, and the activation energy $E = 263.7$ kJ/mol, the universal gas constant $R = 8.314$ J/(mol·K).

2.3. Thermophysical property calculations

The calculation of the density ρ, viscosity μ and thermal conductivity λ for n-decane and each pyrolytic product are based on the extended corresponding states principle. Propane is selected as the reference material, whose state equation adopts 32 parameters Modified Benedict-Webb-Rubin (MBWR) equation.[23] For each species and the mixture, the density is achieved according to the corresponding relation between the species and the reference propane, and the viscosity and the thermal conductivity are derived from the TRAnsport Property Prediction (TRAPP) method,[24] and the thermal capability c_p is calculated by means of deviation function method.

Fig. 1 shows the density, specific thermal capacity, thermal conductivity and viscosity of n-decane under different supercritical pressures calculated by the methods above and the data of National Institute of Standard and Technology (NIST). Good agreement has been reached between the calculated results and the data of NIST.

2.4. Computational model and mesh

Fig. 2 shows the schematic of the physical model of the flow in a circular tube with the length of $L = 900$ mm and the diameter of $d = 2$ mm. From Fig. 2, it demonstrates a 600 mm heated section enforced with a constant and uniform surface heat flux. At the inlet, a adiabatic section with 150 mm in length is included to ensure a fully developed flow, while at the outlet a adiabatic section with 150 mm in length is adopted to avoid the outflow boundary effects. The computational model is modeled in a 2D axial-symmetric domain. The pyrolysis behavior of n-decane is influenced by the pressure and wall heat flux. The operating pressure ranged from 3 to 5 MPa, with different wall heat fluxes from 1.0 to 1.2 MW/m^2. The inlet temperature was 400 K, and mass flow rate remained constant at 2 g/s. All these geometric parameters and the boundary conditions are relevant to the practical regenerative cooling applications in the scramjet. Meanwhile, special heat transfer characteristics, such as heat transfer deterioration and enhancement, could be well observed under these parameters.

A mesh independence study was conducted to identify an appropriate mesh density for the aimed calculations. In the current work, a set of computational mesh of 900 × 40 in the axial and radial directions has been proved to be sufficient, and the radial mesh is exponentially fined in the near-wall region. Under the current computational conditions, $y+$ of the first near-wall node is kept at approximately 1.0, which is required by the "enhanced wall treatment".

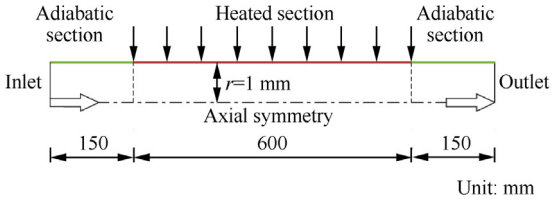

Fig. 2 Schematic of physical model.

3. Results and discussion

3.1. Validation of chemical kinetics model and numerical method

In the current study, the openly published experimental and computational data of Ward et al.[16] were used to validate the developed chemical kinetics model and numerical method. In accordance with the experimental conditions, the tube length and diameter are 0.375 and 0.5 mm respectively. The inlet temperature T_{in} is 473 K, and the outlet pressure p is 3.45 MPa. The mass flow rate ranges from 0.25 to 0.75 mL/min, with different maximum wall temperatures 823 and 873 K. The results of the outlet mass fraction of n-decane with maximum wall temperature $T_w = 873$ K and $T_w = 823$ K are shown in Fig. 3(a). The variations of the bulk fluid temperature and axial velocity along the tube are shown in Fig. 3(b) under the condition of mass flow rate $G = 0.5$ mL/min and $T_w = 873$ K. The outlet mass fraction of n-decane, bulk fluid temperature and axial velocity are defined by Eqs. (10)–(12) respectively.

$$Y_{C_{10}H_{22},f} = \frac{\int_A \rho u Y_{C_{10}H_{22}} dA}{\int_A \rho u dA} \tag{10}$$

$$T_f = \frac{\int_A \rho u c_p T dA}{\int_A \rho u c_p dA} \tag{11}$$

$$u_f = \frac{\int_A \rho u^2 dA}{\int_A \rho u dA} \tag{12}$$

where A is the cross-section area of the tube.

As shown in Fig. 3, it can be seen clearly that the comparison between the numerical results and the existing data has a good agreement. It should be pointed out that the second-order pyrolysis will take place in the actual situation when the n-decane conversion becomes larger. As a result, the n-decane conversion is overestimated by the computation with one global reaction model.[16] In order to reduce the error that is caused by considering the second-order pyrolysis, the n-decane mass fractions of all the cases in this study are above 0.6.

3.2. Influence factors to pyrolysis behavior

Fig. 4 show the distribution of n-decane conversion along the heated section of the tube under the pressure of 5 and 3 MPa respectively. The heated section is under three different wall heat fluxes of $q = 1.0$, 1.1 and 1.2 MW/m^2. In the current work, the n-decane conversion is defined as

$$y = (1 - Y_{C_{10}H_{22},f}) \times 100\% \tag{13}$$

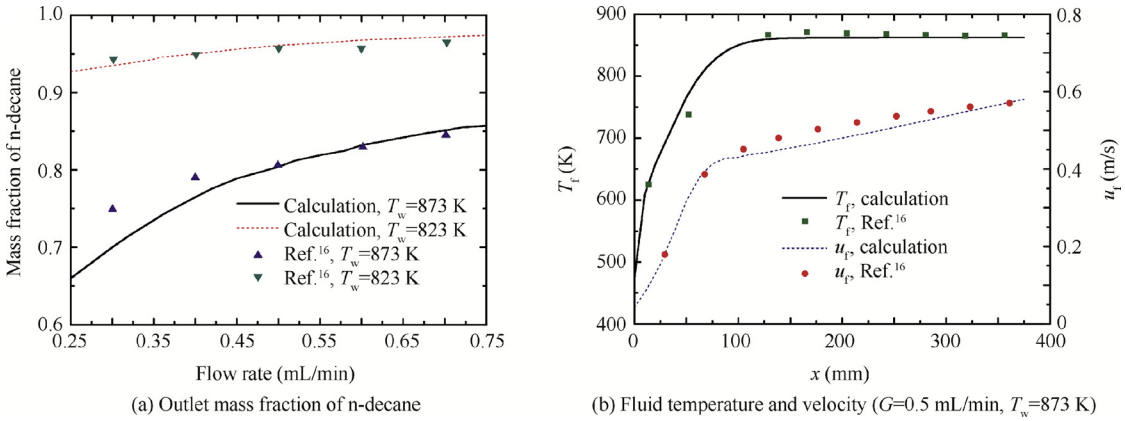

(a) Outlet mass fraction of n-decane (b) Fluid temperature and velocity (G=0.5 mL/min, T_w=873 K)

Fig. 3 Comparison between calculated data and data in Ref.[16] (T_{in} = 473 K, p = 3.45 MPa).

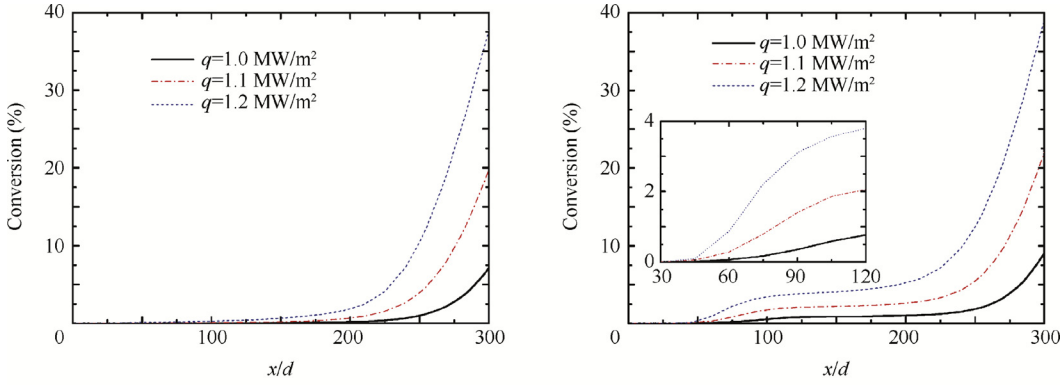

(a) p=5 MPa (b) p=3 MPa

Fig. 4 Distribution of conversion of n-decane under different heat fluxes.

The location at x/d = 0 starts from the beginning of the heated section in the following discussion. As illustrated in Fig. 4(a), the n-decane conversion under 5 MPa maintains close to zero before x/d = 150, since pyrolysis does not normally occur. After x/d = 150, the n-decane conversion starts to increase and increasing rate rises drastically. Fig. 4(b) reveals that n-decane conversion begins to increase at x/d = 45 under 3 MPa. The increasing rate of n-decane conversion tends to slow down from x/d = 100, which is followed by a second rise after x/d = 200, as shown in Fig. 4(b). The n-decane conversion increase at the beginning of the heated section under 3 MPa becomes more obvious when the wall heat flux goes up.

Fig. 5 shows the detailed distribution of temperature and logarithm reaction kinetic rate in the symmetry plane of the heated section under the heat flux of 1.2 MW/m^2. The variation of the temperature near the wall indicates that heat transfer deterioration appears before x/d = 100, and it could be due to the drastic variation of the physical properties.[10,25] As can be seen in Fig. 5(b), the wall temperature reaches about 1100 K before x/d = 100. As the reaction rate is highly sensitive to the temperature, it is the extremely high pyrolysis rate near the wall, which gives rise to n-decane conversion increase at the beginning of the heated section, as shown in Fig. 5(d). As illustrated in Fig. 5, heat transfer deterioration disappears and turns to heat transfer enhancement in the segment of 100 < x/d < 200. The decreased wall temperature reduces the pyrolysis rate near the wall. In addition, pyrolysis would not normally occur with the main stream temperature that is below 750 K. Therefore, the n-decane conversion increases slowly in heat transfer enhanced segment. After x/d = 200, the main stream temperature and pyrolysis rate continuously go up, and accordingly, bring about a sharp rise of the n-decane conversion.

Heat transfer deterioration would be less evident or even disappear with the increasing pressure, as the physical property changes become smaller under a higher pressure.[10,25] Fig. 6 demonstrates the distribution of bulk fluid temperature T_f and wall temperature T_w under 5 and 3 MPa. With a much smaller degree of heat transfer deterioration, the wall temperature under 5 MPa is much lower than that under 3 MPa before x/d = 100. This explains the late increase of n-decane conversion under 5 MPa, in contrast with that under 3 MPa.

It can be also seen from Figs. 4(a) and (b) that the n-decane conversion at x/d = 100 is about 0.5% under 5 MPa and is about 4% under 3 MPa. After x/d = 100, the conversion under 5 MPa increases by 37% and reaches about 37.5% at the end of the heated section, while that under 3 MPa increases by 34.5% and eventually reaches about 38.5%. The fluid temperature reaches 600 K at x/d = 100, as illustrated in Fig. 6. The density decreases slower under 5 MPa than that under 3 MPa when the

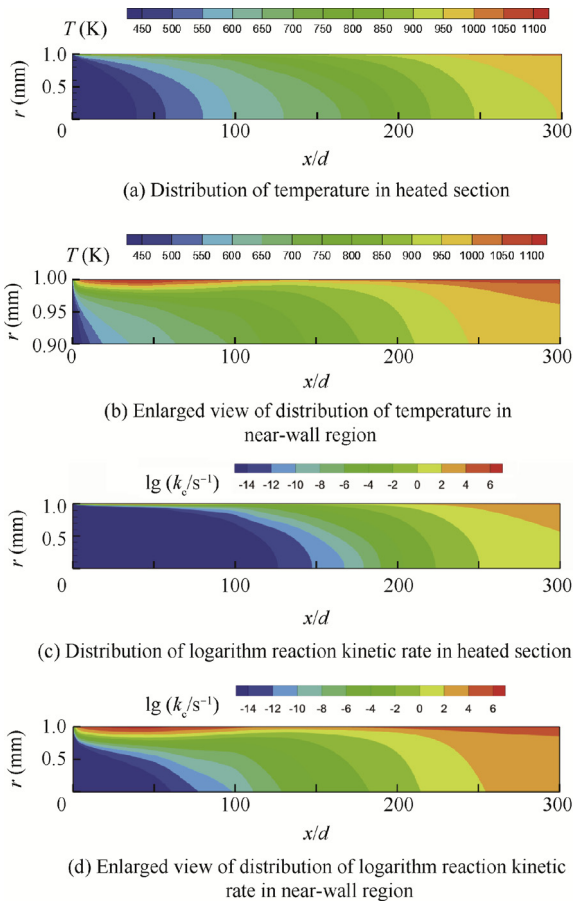

Fig. 5 Distribution of temperature and logarithm reaction kinetic rate (p = 3 MPa, q = 1.2 MW/m^2).

temperature is above 600 K, as shown in Fig. 1(a). As the smaller density gives rise to the larger acceleration, the residence time of the fluid flowing from x/d = 100 to the end of the heated section is shorter under 3 MPa. This accounts for the larger increase of conversion after x/d = 100 under 5 MPa.

3.3. Pyrolysis effects on heat transfer characteristics

Fig. 7 shows the heat transfer performance along the heated section of the tube under the condition of p = 3 MPa, q = 1.2 MW/m^2, and two sets of result, with and without consideration of pyrolysis, are compared. The n-decane conversion results in this case can be referred to from Fig. 4(b). Fig. 7(a) shows the distribution of the bulk fluid temperature and the wall temperature, and Fig. 7(b) shows the distribution of the heat transfer coefficient which is defined as

$$h = \frac{q}{T_w - T_f}$$

As illustrated in Fig. 7, at the beginning of the heated section, the increase of the heat transfer coefficient with pyrolysis occurs much earlier than that without pyrolysis. Accordingly, pyrolysis shortens the heat transfer deteriorated segment and lowers the maximum value of the wall temperature. After x/d = 150, the results with pyrolysis deviate from the results without pyrolysis, due to the increasing amount of reacted

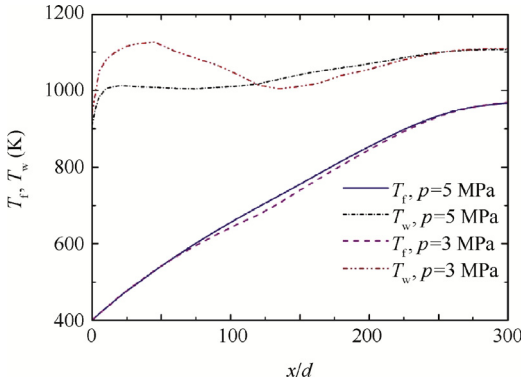

Fig. 6 Distribution of bulk fluid temperature and wall temperature under 5 and 3 MPa (q = 1.2 MW/m^2).

n-decane. The higher heat transfer coefficient and the lower fluid bulk temperature with pyrolysis make the wall temperature much lower than that without pyrolysis. As shown in Fig. 7(a), the fluid temperature and wall temperature are reduced by 90 and 110 K at the end of the heated section respectively.

Figs. 8 and 9 show the detailed distribution of the physical properties and velocity in the symmetry plane of the heated section with and without pyrolysis respectively, under the same condition of Fig. 7. As the tube flow is heated up, the temperature near the wall quickly exceeds the pseudo-critical temperature. Because of the descending density and specific thermal capacity, the heat capacity near the wall decreases, which would lower the heat transfer capability and lead to extremely high temperature near the wall.[10,25,26] After the flow is further heated up, the increasing bulk temperature leads to the growth of velocity. The increased flow velocity causes the recovery of the coolant capability, and consequently enhances the heat transfer process.[10,25] As revealed by the comparison between Figs. 8 and 9, pyrolysis brings about little change in thermal conductivity, and makes the fluid heat capacity lower due to the increasing proportions of the small molecule productions. However, the heat transfer process with pyrolysis is less deteriorated before x/d = 150 and much more enhanced after x/d = 150, as shown in Fig. 7. This indicates that the further fluid acceleration caused by pyrolysis plays the dominant role in convective heat transfer. Figs. 8(c) and 9(c) demonstrate the larger velocity with pyrolysis. At the end of the heated section, the flow velocity without pyrolysis is about 13 m/s, while that with pyrolysis reaches 20 m/s. It is the larger velocity with pyrolysis that leads to the higher heat transfer coefficient.

As revealed from the results under heat fluxes of q = 1.0, 1.1 MW/m^2 in Fig. 10 and q = 1.2 MW/m^2 in Fig. 7, pyrolysis shortens the heat transfer deteriorated segment and lowers the temperature maximum to a larger extent, as the heat flux becomes greater. The temperature maximum without pyrolysis rises from 1051 to 1167 K, while that with pyrolysis rises from 1030 to 1126 K when the heat flux increases from 1.0 to 1.2 MW/m^2. After x/d = 150, the wall temperature tends to be constant at the end of the heated section as the heat flux becomes greater. It can be explained by the fact that the greater heat flux could lead to larger conversion which restrains the fluid temperature from going up and enhances the convective heat transfer. The temperature reached at the

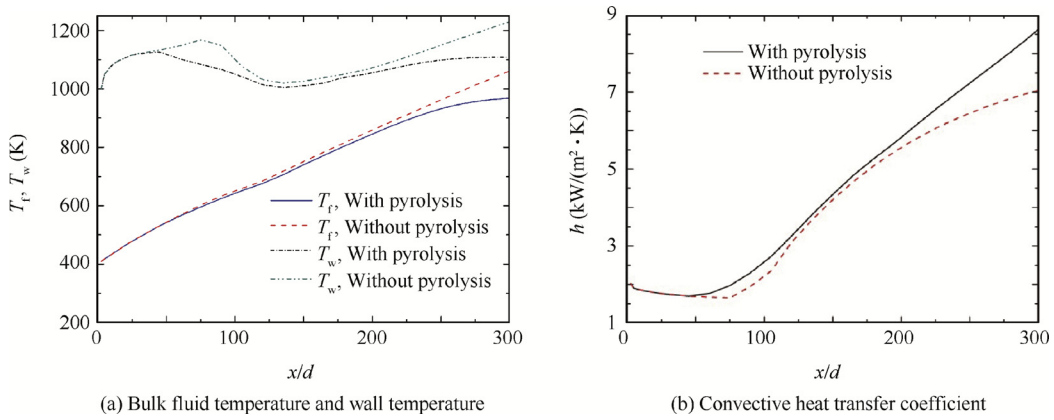

(a) Bulk fluid temperature and wall temperature (b) Convective heat transfer coefficient

Fig. 7 Heat transfer characteristics with/without pyrolysis (p = 3 MPa, q = 1.2 MW/m^2).

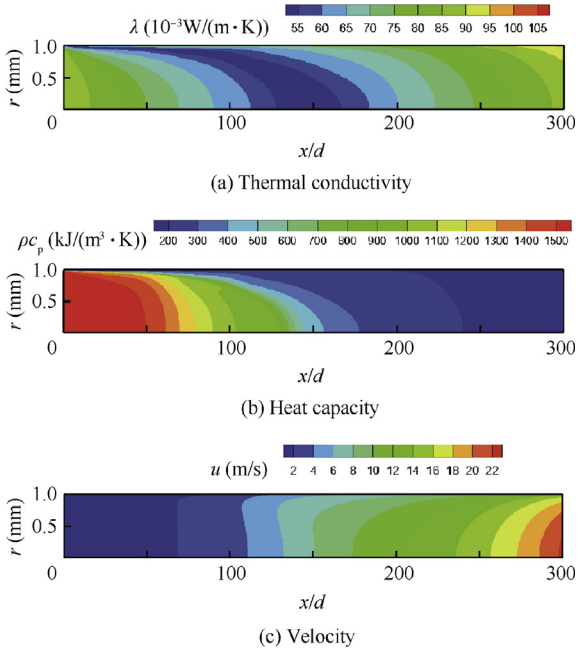

Fig. 8 Distribution of physical properties and velocity with pyrolysis (p = 3 MPa, q = 1.2 MW/m^2).

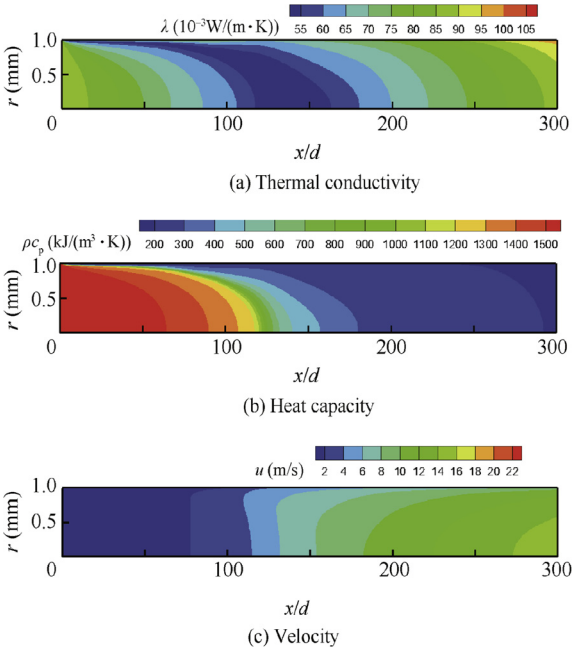

Fig. 9 Distribution of physical properties and velocity without pyrolysis (p = 3 MPa, q = 1.2 MW/m^2).

end of the heated section without pyrolysis rises from 1118 to 1230 K, whereas that with pyrolysis rises from 1081 to 1109 K when the heat flux increases from 1.0 to 1.2 MW/m^2. From the above analysis, it can be concluded that pyrolysis is conducive for the cooling structure to withstand a higher heat flux under a certain temperature allowed by solid material.

3.4. Pyrolysis effects on flow resistance

It is well known that friction on the tube wall causes pressure drop along the axial direction. The axial pressure gradient can be used to indicate the flow resistance, seen in Eq. (14):

$$\left|\frac{\mathrm{d}p}{\mathrm{d}x}\right| = f\frac{1}{d}\cdot\frac{\rho u^2}{2} = f\frac{G}{2A}\cdot u \tag{14}$$

where f is the resistance coefficient.

Fig. 11(a) shows the distribution of axial pressure gradient under the condition of p = 5 MPa, q = 1.2 MW/m^2 with and without pyrolysis. The pressure gradient without pyrolysis has little variation after x/d = 150, while that with pyrolysis begins to increase abruptly. As discussed in detail in the previous study[11], the dramatic variation of supercritical fluid density plays the dominant role in pressure drop. As can be clearly seen from Fig. 11(b), the further reduced density caused by pyrolysis leads to larger acceleration. The greater radial velocity gradient near the wall enlarges the shear stress and friction at the wall. That explains why pressure gradient increases abruptly and becomes different from that without pyrolysis.

Fig. 12(a) shows the distribution of axial pressure gradient under the condition of p = 3 MPa, q = 1.2 MW/m^2 with and without pyrolysis. In contrast with the case under 5 MPa, the differences caused by pyrolysis begin to appear at x/d = 45,

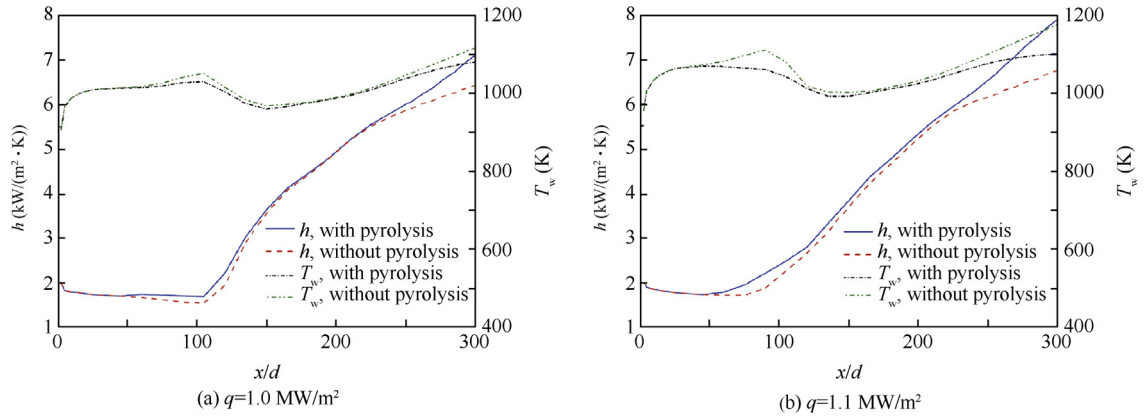

Fig. 10 Heat transfer characteristics with and without pyrolysis under different heat fluxes (p = 3 MPa).

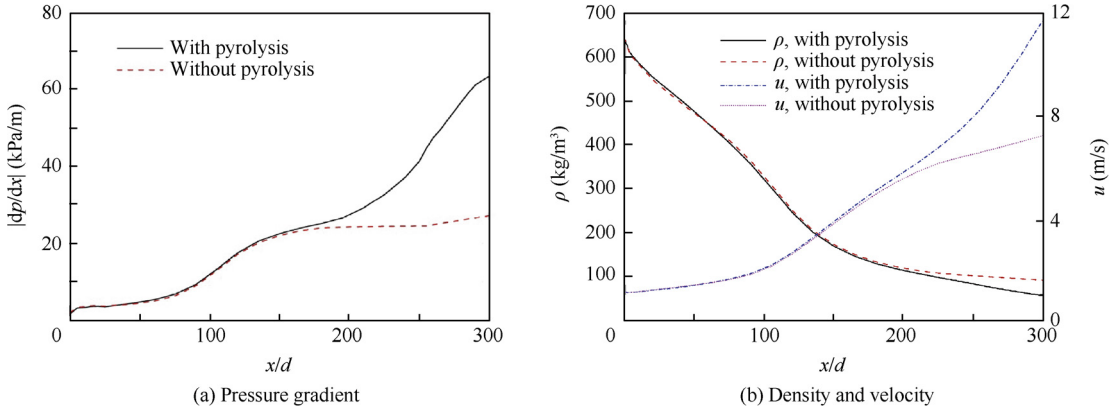

Fig. 11 Distribution of axial pressure gradient, velocity and density with and without pyrolysis (p = 5 MPa, q = 1.2 MW/m^2).

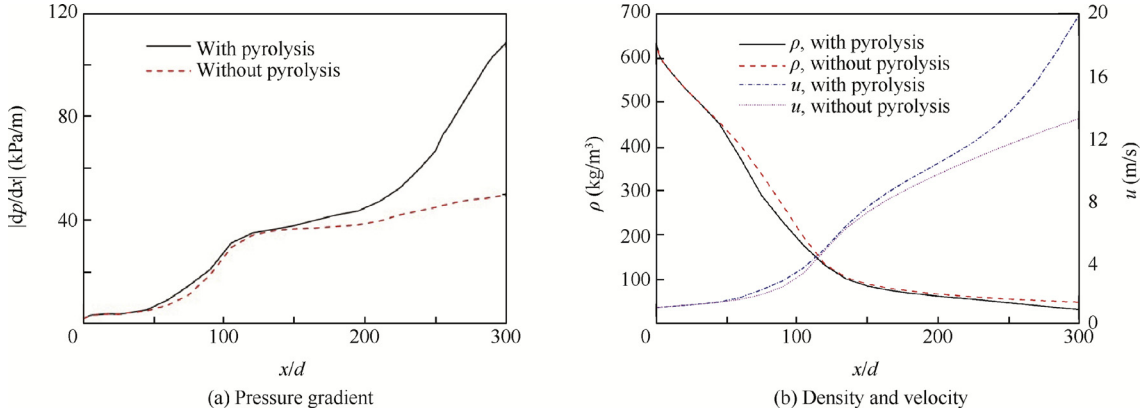

Fig. 12 Distribution of axial pressure gradient, velocity and density with and without pyrolysis (p = 3 MPa, q = 1.2 MW/m^2).

and pressure gradient with pyrolysis is little greater in the section from x/d = 45 to 105. This results from the earlier occurrence of pyrolysis, which leads to a more rapid acceleration in this section, as shown in Fig. 12(b). Moreover, the value of pressure gradient under 3 MPa is much greater than that under 5 MPa, attributing to the lower density and higher velocity under 3 MPa.

4. Conclusions

In this paper, a numerical investigation of n-decane flow and heat transfer coupled with pyrolysis is conducted. The heat transfer and the pyrolysis process under supercritical pressure, as well as the mechanism of pyrolysis effects on heat transfer characteristics and flow resistance, are discussed and analyzed

in detail. Based on the results of the current research, the following specific conclusions may be made:

(1) The pyrolytic reaction rate is highly sensitive to the temperature, and therefore, the n-decane conversion arises rapidly as the fluid temperature becomes high enough after $x/d = 150$. The n-decane conversion before $x/d = 150$ remains nearly to be 0 under 5 MPa, but has an increment under 3 MPa. This contrast is caused by the heat transfer deterioration under 3 MPa.
(2) Pyrolysis gives rise to a further decrease in fluid density, which leads to a further acceleration. The enhanced heat transfer and the lower fluid temperature jointly slow the rise of wall temperature, and the value of the wall temperature is much lower than that without pyrolysis.
(3) Fluid acceleration plays the dominant role in heat transfer enhancement. Pyrolysis in the heat transfer deteriorated segment makes the fluid velocity higher, which results in an earlier rise of the heat transfer coefficient. As a consequence of this, pyrolysis shortens the heat transfer deteriorated segment and lowers the temperature maximum.
(4) The further acceleration of fluid caused by pyrolysis plays an important role in bringing about much greater flow resistance. Attributing to the higher velocity, pressure gradient increases abruptly as pyrolysis takes place after $x/d = 150$.

Acknowledgement

The authors gratefully acknowledge the funding support from Program for National Natural Science Foundation of China (No. 51406005).

References

1. Edwards T. Liquid fuels and propellants for aerospace propulsion: 1903–2003. *J Propul Power* 2003;**19**(6):1089–107.
2. Sobel DR, Spadaccini LJ. Hydrocarbon fuel cooling technologies for advanced propulsion. *J Eng Gas Turbines Power* 1997;**119**(2):344–51.
3. Gascoin N, Abraham G, Gillard P. Synthetic and jet fuels pyrolysis for cooling and combustion applications. *J Anal Appl Pyrolysis* 2010;**89**(2):294–306.
4. Dewitt MJ, Edwards T, Shafer L, Brooks D, Striebich R, Bagley SP. Effect of aviation fuel type on pyrolytic reactivity and deposition propensity under supercritical conditions. *Ind Eng Chem Res* 2011;**50**(18):10434–51.
5. Edwards T. Cracking and deposition behavior of supercritical hydrocarbon aviation fuels. *Combust Sci Technol* 2006;**178**(1–3):307–34.
6. Hua YX, Wang YZ, Meng H. A numerical study of supercritical forced convective heat transfer of n-heptane inside a horizontal miniature tube. *J Supercrit Fluids* 2010;**52**(1):36–46.
7. Zhou WX, Bao W, Qin J. Deterioration in heat transfer of endothermal hydrocarbon fuel. *J Therm Sci* 2011;**20**(2):173–80.
8. Deng HW, Zhu K, Xu GQ, Tao Z, Sun JN. Heat transfer characteristics of hydrocarbon fuel at supercritical pressure in vertical circular tubes. *J Enhance Heat Transf* 2012;**27**(3):595–603.
9. Zhang CB, Xu GQ, Gao L, Tao Z, Deng HW, Zhu K. Experimental investigation on heat transfer of a specific fuel (RP-3) flows through downward tubes at supercritical pressure. *J Supercrit Fluids* 2012;**72**(9):90–9.
10. Urbano A, Nasuti F. Conditions for the occurrence of heat transfer deterioration in light hydrocarbons flows. *Int J Heat Mass Transf* 2013;**65**(5):599–609.
11. Zhu JQ, Tao Z, Deng HW, Wang K, Yu X. Numerical investigation of heat transfer characteristics and flow resistance of kerosene RP-3 under supercritical pressure. *Int J Heat Mass Transf* 2015;**91**:330–41.
12. Liu B, Zhu YH, Yan JJ, Lei YT, Zhang B, Jiang PX. Experimental investigation of convection heat transfer of n-decane at supercritical pressures in small vertical tubes. *Int J Heat Mass Transf* 2015;**91**:734–46.
13. Yu J, Eser S. Thermal decomposition of C10–C14 normal alkanes in nearcritical and supercritical regions: product distributions and reaction mechanisms. *Ind Eng Chem Res* 1997;**36**(3):574–85.
14. Yu J, Eser S. Kinetics of supercritical-phase thermal decomposition of C10–C14 normal alkanes and their mixtures. *Ind Eng Chem Res* 1997;**36**(3):585–91.
15. Herbinet O, Marquaire PM, Battin-Leclerc F, Fournet R. Thermal decomposition of n-dodecane: experiments and kinetic modeling. *J Anal Appl Pyrolsis* 2007;**78**(2):419–29.
16. Ward TA, Ervin JS, Striebich RC, Zabarnick S. Simulations of flowing mildly-cracked normal alkanes incorporating proportional product distributions. *J Propul Power* 2004;**20**(3):394–402.
17. Ward TA, Ervin JS, Zabarnick S, Shafer L. Pressure effects on flowing mildly-cracked n-decane. *J Propul Power* 2005;**21**(2):344–55.
18. Zhu YH, Liu B, Jiang PX. Experimental and numerical investigation on n-decane thermal cracking at supercritical pressures in a vertical tube. *Energy Fuels* 2013;**28**(1):466–74.
19. Zhou WX, Jia ZJ, Qin J, Bao W, Yu B. Experimental study on effect of pressure on heat sink of n-decane. *Chem Eng J* 2014;**243**(4):127–36.
20. Zhao GZ, Song WY, Zhang RL. Effect of pressure on thermal cracking of china RP-3 aviation kerosene under supercritical conditions. *Int J Heat Mass Transf* 2015;**84**:625–32.
21. Xu KK, Meng H. Modeling and simulation of supercritical-pressure turbulent heat transfer of aviation kerosene with detailed pyrolytic chemical reactions. *Energy Fuels* 2015;**29**(7):4137–49.
22. Ruan B, Meng H, Yang V. Simplification of pyrolytic reaction mechanism and turbulent heat transfer of n-decane at supercritical pressures. *Int J Heat Mass Transf* 2014;**69**(2):455–63.
23. Younglove BA, Ely JF. Thermophysical properties of fluids. II. Methane, ethane, propane, isobutane, and normal butane. *J Phys Chem Ref Data* 1987;**16**(4):577–798.
24. Huber ML. *Transport properties of fluids, the correlation, prediction and estimation*. Cambridge: Cambridge University Press; 1996. p. 497–501.
25. Urbano A, Nasuti F. Onset of heat transfer deterioration in supercritical methane flow channels. *J Thermophys Heat Transf* 2013;**27**(27):298–308.
26. Wang YZ, Hua YX, Meng H. Numerical studies of supercritical turbulent convective heat transfer of cryogenic-propellant methane. *J Thermophys Heat Transf* 2010;**24**(3):490–500.